SWI/SNF regulates a transcriptional programme that induces senescence to prevent liver cancer

Luca Tordella[1,2,+], Sadaf Khan[1,2,+], Anja Hohmeyer[3], Ana Banito[1,2], Sabrina Klotz[3], Selina Raguz[1,2], Nadine Martin[1,2,#], Gopuraja Dhamarlingam[1,2], Thomas Carroll[1,2], José Mario González Meljem[4], Sumit Deswal[5], Juan Pedro Martínez-Barbera[4], Ramón García-Escudero[6,7], Johannes Zuber[5], Lars Zender[3] and Jesús Gil[1,2,*]

[1]MRC Clinical Sciences Centre (CSC), Du Cane Road, London W12 0NN.
[2]Institute of Clinical Sciences (ICS), Faculty of Medicine, Imperial College London, Du Cane Road, London W12 0NN
[3]Division of Molecular Oncology of Solid Tumours, Dept. of Internal Medicine I, Eberhard Karls University Tübingen, 72076 Tübingen, Germany.
[4]Developmental Biology and Cancer Programme, Birth Defects Research Centre, UCL Institute of Child Health, London WC1N 1EH, UK.
[5]Research Institute of Molecular Pathology (IMP), Dr. Bohr-Gasse 7, 1030 Vienna, Austria.
[6]Molecular Oncology Unit, CIEMAT (ed70A), 28040 Madrid, Spain.
[7]Biomedical Research Institute I+12, Univ. Hosp. 12 de Octubre, 28041 Madrid, Spain.
[#]Current address: Senescence Escape Mechanisms Laboratory, UMR INSERM 1052 CNRS 5286, Centre de Recherche en Cancérologie de Lyon, Lyon, France

[+]Co-first author.

*Corresponding author: jesus.gil@csc.mrc.ac.uk

Short title: ARID1B regulates senescence to prevent cancer

Key words: Senescence; ARID1B; SWI/SNF; p53; ENTPD7; dNTP metabolism; cancer.

ABSTRACT

Oncogene-induced senescence (OIS) is a potent tumour suppressor mechanism. To identify senescence regulators relevant to cancer, we screened an shRNA library targeting genes deleted in hepatocellular carcinoma (HCC). Here, we describe how knockdown of the SWI/SNF component ARID1B prevents OIS and cooperates with RAS to induce liver tumours. ARID1B controls $p16^{INK4a}$ and $p21^{CIP1a}$ transcription but also regulates DNA damage, oxidative stress and p53 induction, suggesting that SWI/SNF uses additional mechanisms to regulate senescence. To systematically identify SWI/SNF targets regulating senescence, we carried out a focused shRNA screen. We discovered several new senescence regulators including ENTPD7, an enzyme that hydrolyses nucleotides. ENTPD7 affects oxidative stress, DNA damage and senescence. Importantly, expression of ENTPD7 or inhibition of nucleotide synthesis in ARID1B-depleted cells results in re-establishment of senescence. Our results identify novel mechanisms by which epigenetic regulators can affect tumor progression and suggest that pro-senescence therapies could be employed against SWI/SNF-mutated cancers.

INTRODUCTION

The extensive sequencing of cancer genomes has provided a comprehensive list of the recurrent genetic alterations observed in different tumour types. In addition to well-known oncogenes and tumour suppressors, these studies have linked unforeseen candidates to cancer (Watson et al. 2013). In parallel, our overall understanding of cancer biology has advanced considerably and specific hallmarks have been proposed to explain the diversity of cancer (Hanahan and Weinberg 2011). However, despite progress in both areas, the explanation for the functional significance that recurring genetic alterations have in cancer progression is often missing, but much needed to develop targeted therapies.

Bypass of senescence is a common characteristic of advanced tumours (Narita and Lowe 2005). In response to oncogenic signalling, cells activate a stress response termed oncogene-induced senescence (OIS). OIS is a feature of pre-malignant lesions and has an important role in tumour suppression (Collado and Serrano 2010). Consequently, advanced tumours almost invariably escape senescence and this constitutes one of the hallmarks of cancer (Hanahan and Weinberg 2011). A well-studied example is hepatocellular carcinoma (HCC). Aberrant oncogenic activation in hepatocytes activates OIS that in turn limits HCC generation via cell-intrinsic and -extrinsic mechanisms (Kang et al. 2011). Overall, OIS is a complex programme that includes the implementation of a highly stable cell cycle arrest but also profound changes in transcription, metabolism, secretome and chromatin organization (Kuilman et al. 2010). Many of these senescent phenotypes are under epigenetic control (Barradas et al. 2009, and Kia et al. 2009). Interestingly, a major discovery from cancer genome studies is that chromatin modifiers are often mutated

in cancer (Plass et al. 2013). In particular, genes encoding for components of the SWI/SNF chromatin-remodelling complex are frequently deleted or mutated across a wide spectrum of cancers (Kadoch et al. 2013). This suggests that SWI/SNF plays a fundamental protective role towards tumourigenesis via the regulation of basic cellular functions. Whether the frequency of these alterations relates to the ability of the SWI/SNF complex to control senescence is an enticing possibility.

The SWI/SNF complexes reposition nucleosomes and bind to DNA-regulatory regions to control transcription. Loss of function mutations of different SWI/SNF components drive tumourigenesis by disrupting gene expression (Wilson and Roberts 2011). SWI/SNF are macromolecular complexes comprising 12-15 subunits: a catalytic ATPase subunit, SMARCA4/BRG1 or SMARCA2/BRM and several core subunits, such as SMARCB1/SNF5/INI1/BAF47 or SMARCC1/BAF155 are common to all SWI/SNF complexes. Other subunits, such as ARID1A and ARID1B are mutually exclusive components of BAF (BRG1-associated factor) complexes, while PBRM1 and ARID2 are specific for PBAF (polybromo BRG1-associated factor) complexes (Helming et al. 2014a).

Many components of SWI/SNF complexes are altered in different malignancies, adding up to a global ~20% of cancers bearing mutations in SWI/SNF genes (Kadoch et al. 2013). The BAF subunit ARID1A has the highest mutation rate amongst SWI/SNF components (Helming et al. 2014a). Mutations in its paralog ARID1B are less frequent but have also been observed in melanoma, gastric, colorectal, HCC, neuroblastoma and pancreatic cancer (Fujimoto et al. 2012; Khursheed et al. 2013; Sausen et al. 2013; Lee et al. 2015). In HCC, more than 20% of the tumours present alterations in SWI/SNF components, and mutations in ARID1B are second in frequency only to ARID1A (Fujimoto et al. 2012).

Given the prevalence of SWI/SNF mutations, several studies have investigated the molecular mechanisms linking SWI/SNF disruption with cancer progression. SWI/SNF components have been reported to interact with RB (Trouche et al. 1997), MYC (Cheng et al. 1999), or p53 (Lee et al. 2002). Moreover, inactivation of the SWI/SNF complex due to loss of specific components such as SNF5, BRD7 or PBR1 results in senescence bypass (Oruetxebarria et al. 2004; Burrows et al. 2010; Drost et al. 2010). Direct transcriptional regulation of $p16^{INK4a}$ (Oruetxebarria et al. 2004; Kia et al. 2008) or $p21^{CIP1}$ (Chai et al. 2005) by SWI/SNF complexes might explain in part their role in senescence. However, a more comprehensive explanation of how SWI/SNF regulates senescence, and how this is relevant for tumourigenesis is still lacking.

In this investigation, we carried out a functional screen to identify HCC-deleted genes regulating senescence. We found that depletion of ARID1B blunted the senescence response and cooperated with oncogenic Ras in HCC formation. By systematically investigating ARID1B target genes, we discovered several novel mediators of senescence, amongst them ENTPD7, an enzyme involved in nucleotide metabolism. Overall, the identification of novel mechanisms by which ARID1B loss restricts senescence could reveal vulnerabilities (e.g. nucleotide metabolism) useful to target cancers bearing mutations in SWI/SNF genes.

RESULTS

An shRNA screen identifies *ARID1B* as a regulator of senescence.

Senescence is a potent tumour suppressor mechanism (Kuilman et al. 2010) often disabled in cancer cells (Hanahan and Weinberg 2011). For example, induction of senescence in preneoplastic hepatocytes actively prevents hepatocellular carcinoma (HCC) (Kang et al. 2011). To identify tumour suppressors that control senescence and could limit liver cancer, we devised a genetic screen using an shRNA library targeting genes frequently deleted in HCC (Zender et al. 2008). We carried out the screen in mouse embryonic fibroblasts (MEFs), which are a robust system previously used to identify regulators of senescence (Jacobs et al. 2000; Kondoh et al. 2005). MEFs were infected with the shRNA library, selected and passaged regularly until controls underwent senescence (Fig. 1A; Supplemental Fig. S1A). The relative distribution of shRNAs during the screen was determined using next generation sequencing (NGS). We then used statistical analysis to identify shRNAs significantly enriched in MEFs bypassing senescence (Fig. 1B; Supplemental Fig. S1B). Amongst the enriched shRNAs, two targeted the SWI/SNF subunit *Arid1b* (including the top shRNA enriched in the screen, Fig. 1B; Supplemental Fig. S1B). Since SWI/SNF components are frequently mutated or deleted in cancer (Oruetxebarria et al. 2004; Shain and Pollack 2013), we decided to confirm that *Arid1b* knockdown prevented senescence using two shRNAs targeting murine *Arid1b* (Fig. 1C; Supplemental Fig. S1C,D). Similarly to what we observed when using an shRNA targeting *Ink4a/Arf* (shp16/Arf, Fig. S1C), knockdown of *Arid1b* blunted replicative senescence, as evidenced by increased colony formation, higher percentage of cells incorporating BrdU and a decrease in

the percentage of senescence-associated β-galactosidase (SA-β-Gal) positive cells when compared to control MEFs (Fig. 1C). Additionally, we tested whether knockdown of Arid1b expression protected MEFs against senescence induced by oncogenic RAS. While MEFs expressing RAS^{G12V} underwent premature senescence, MEFs infected with shRNAs targeting Arid1b or p53 continued to proliferate (Supplemental Fig. S1E). Moreover, the cells grew anchorage-independently, as assessed by soft-agar assay, indicating oncogenic cooperation between RAS^{G12V} and Arid1b knockdown (Fig. 1D). Altogether these results suggest that knockdown of Arid1b enables bypass of senescence in MEFs.

Knockdown of Arid1b cooperates in HCC generation by blunting OIS.

Next, we investigated whether Arid1b depletion can prevent senescence *in vivo* and in this way contribute to liver cancer development. To test this, we used a mouse model in which OIS is triggered in hepatocytes via transposon-mediated transfer of oncogenic Nras ($Nras^{G12V}$) delivered by hydrodynamic tail vein (HDTV) injection (Kang et al. 2011) (Fig. 2A). In this model, the senescent hepatocytes activate an immune response that results in their gradual elimination (Kang et al. 2011). To investigate whether Arid1b knockdown affects OIS *in vivo*, we co-expressed $Nras^{G12V}$ and either control or Arid1b-targeting shRNAs. We measured Arid1b levels in $Nras^{G12V}$ expressing hepatocytes nine days after transposon injection. Hepatocytes expressing an inactive variant ($Nras^{G12V,D38A}$) displayed lower levels of Arid1b than those carrying the constitutively active variant ($Nras^{G12V}$), indicating that oncogenic $Nras^{G12V}$ induces Arid1b expression during senescence *in vivo*. Furthermore both shRNAs targeting Arid1b blunted its induction (Fig. 2B; Supplemental Fig. S2A,B). We next evaluated the consequences of depleting Arid1b

in Nras-expressing hepatocytes. At day 9, there were more Nras positive hepatocytes present in the livers of mice transduced with $Nras^{G12V}$_shArid1b than $Nras^{G12V}$_shCTR vectors (Fig. 2C,D). The higher percentage of $Nras^{+}$ hepatocytes correlated with reduced senescence as shown by decreased levels of SA-β-Gal in the livers of mice transduced with $Nras^{G12V}$_shArid1b vectors. In addition, a lower percentage of Nras positive hepatocytes were also positive for $p21^{Cip1a}$ or $p16^{Ink4a}$ upon Arid1b depletion (Fig. 2C,D). Other SWI/SNF components have been suggested to control senescence by regulating $p21^{Cip1a}$ or $p16^{Ink4a}$ transcription (Chai et al. 2005). Interestingly, we also observed a decreased DNA damage response (DDR, assessed by 53BP1 staining) in $Nras^{+}$ hepatocytes of mice transduced with $Nras^{G12V}$_shArid1b vectors (Fig. 2E; Supplemental Fig. S2C), suggesting that there might be additional mechanisms by with Arid1b and by extension the SWI/SNF complex control senescence.

$Nras^{+}$ hepatocytes in which Arid1b expression was knocked down also proliferated more, displaying a higher percentage of $Ki67^{+}$ cells (Fig. 2F; Supplemental Fig. S2D). Since depletion of Arid1b blunted the senescence response *in vivo* and resulted in higher percentages of proliferating $Nras^{+}$ hepatocytes, we investigated whether the knockdown of Arid1b cooperated with $Nras^{G12V}$ in tumour formation. To test this, we used a similar protocol as before and monitored the mice regularly for tumour formation (Fig. 2G, left). While only 1/10 mice injected with the Nras_shCTR vector died of tumours during the time they were monitored, 8/13 of those bearing the $Nras^{G12V}$_shArid1b.1 construct succumbed to HCCs (Fig. 2G, middle). Fluorescence imaging confirmed that these tumours derived from hepatocytes expressing the transduced vectors, as they were GFP positive (Fig. 2G, right).

Altogether these results indicate that knockdown of Arid1b contributes to HCC formation by blunting senescence.

ARID1B regulates OIS in human fibroblasts.

To investigate the mechanism by which ARID1B controls senescence in more detail, we took advantage of IMR90 human fibroblasts, as they are a widely-used system to study senescence and are amenable to mechanistic dissection. First we checked whether ARID1B is necessary for the implementation of senescence in human cells. To this end, we generated two shRNAs to target human ARID1B (Supplemental Fig. S3A,B) and used them to infect IMR90 human fibroblasts expressing ER:RAS (IMR90 ER:RAS), an inducible model of OIS. Depletion of ARID1B in IMR90 ER:RAS cells blunted OIS, as evidenced by increased proliferation and a decrease in the percentage of cells positive for SA-β-Gal (Fig. 3A). To investigate how the depletion of ARID1B affects OIS, we performed transcriptional profiling of IMR90 ER:RAS cells infected with an shRNA targeting ARID1B (Fig. 3B, left). Using gene set enrichment analysis (GSEA), a signature of OIS was found significantly downregulated upon ARID1B knockdown (Fig. 3B, middle). GSEA and ingenuity pathway analysis (IPA) showed that SWI/SNF (SMARCA4) target genes were induced during OIS and this induction was blunted by ARID1B knockdown (Fig. 3B, right and data not shown). Interestingly, IPA analysis also suggested that ARID1B depletion prevented the activation of the p53 pathway and oxidative stress observed during OIS (Fig. 3B, right). Key effectors of senescence such as $p16^{INK4a}$ and $p21^{CIP1}$ were downregulated at both mRNA and protein level upon ARID1B depletion (Fig. 3C,D; Supplemental Fig. S3C). Consistent with the observations *in vivo*, depletion of ARID1B resulted in reduced DDR (Fig. 3C,D). In addition, confirming

the IPA analysis, ARID1B knockdown resulted in decreased levels of p53 and oxidative stress (as measured by 8-oxodG staining) (Fig. 3C,D).

ARID1B expression triggers a senescent-like arrest.

To complement the knockdown studies we analysed the effect of expressing ARID1B in IMR90 cells. Expression of ARID1B in IMR90 cells induced growth arrest, SA-β-Gal activity and a decrease in the percentage of BrdU-positive cells (Fig. 4A and Supplemental Fig. S4A). By analysing the transcriptional profiles of IMR90 cells infected with a control vector or ARID1B by GSEA we observed that ARID1B overexpression was associated with signatures of OIS and senescence-related phenotypes such as SASP and cell cycle arrest (Supplemental Fig. S4B). IPA confirmed that ARID1B expression resulted in the upregulation of SWI/SNF target genes and the induction of the DDR and p53 (Fig. 4B,C). Indeed, the expression of ARID1B not only induced $p16^{INK4a}$ and $p21^{CIP1a}$, but also upregulated p53 levels, caused DNA damage and oxidative stress (Fig. 4D,E). We then interrogated the relative contribution of these pathways to the ARID1B-mediated arrest using shRNAs. The arrest caused by ARID1B was prevented partially when the expression of $p16^{INK4a}$ or $p21^{CIP1a}$ had been knocked down (Fig. 4F; Supplemental Fig. S4C). Interestingly, knocking down p53 prevented to a bigger extent the arrest caused by ARID1B expression (Fig. 4F), suggesting an important role of the p53 pathway in ARID1B-mediated arrest. Altogether these observations reinforce the idea that in addition to regulate $p16^{INK4a}$ and $p21^{CIP1}$ transcription, ARID1B uses additional mechanisms, such as the generation of p53-activating stress signals (DDR and oxidative stress), to control senescence.

Identification of novel ARID1B targets controlling senescence.

To identify novel mechanisms by which ARID1B and by extension the SWI/SNF complex, regulate senescence, we generated an shRNA library targeting 255 genes upregulated during OIS. It included a subset of ARID1B-dependent genes, based on our gene expression analysis (Supplemental Fig. S5A). We designed up to 6 shRNAs targeting each gene and cloned the library in a miRE-based vector that has improved knock down efficiency when compared with other shRNA vectors (Fellmann et al. 2013). Using this library, we carried out a screen for bypass of OIS in IMR90 ER:RAS cells (Fig. 5A; Fig. S5B). After infection with the library or controls, senescence was induced by adding 4OHT to activate ER:RAS, and cells were passaged until growth (indicative of senescence bypass) was observed in library-infected plates. The distribution of shRNAs at different time points was calculated by NGS. Importantly, by including up to 6 shRNAs targeting each gene in the library, we were able to analyse the results of the screen at gene rather than shRNA level. Statistical analysis using EdgeR unveiled 14 genes whose shRNAs were significantly enriched ($p<0.001$) in cells bypassing OIS. Interestingly, 13 of the 14 candidates identified in the screen were ARID1B-dependent genes (Supplemental Fig. S5C). Using IPA, we independently confirmed a significant enrichment for SWI/SNF (SMARCA4) target genes among the top hits of the screen (Supplemental Fig. S5D) and for genes related to p53 and ROS (Supplemental Fig. S5D). The top gene identified in the screen was *CDKN1A* (Fig. 5B; Supplemental Fig. S5E), which encodes for $p21^{CIP1}$, a key senescence regulator. Our data and the literature (Chai et al. 2005) support an important role for $p21^{CIP1a}$ in implementing SWI/SNF-mediated senescence. This served as an internal control and confirmed the validity of our approach. Amongst the other genes identified, at least 3

(SLC31A2, ENTPD7 and NDST2) could be functionally associated with the generation of oxidative stress or DDR. We confirmed that these three genes were SWI/SNF targets induced during OIS (Supplemental Fig. S5F-H). To investigate the role of SLC31A2, NDST2 and ENTPD7 in OIS, we generated 2 shRNAs targeting each gene (Supplemental Fig. S6A). Knocking down either ENTPD7, SLC31A2 or NDST2 in IMR90 ER:RAS cells did not affect the strength of RAS/ERK activation (Supplemental Fig. S6B) but prevented the senescent arrest (Fig. 5C,D) and blunted $p21^{CIP1a}$ induction (Fig. 5E). Similarly, depletion of ENTPD7, SLC31A2 or NDST2 partially prevented the senescent arrest caused by ARID1B expression (Supplemental Fig. S6C,D). These results confirm the identification of novel mediators of the effects of ARID1B on OIS.

Multiple ARID1B target genes mediate induction of OIS in the liver.

We next analysed whether the ARID1B targets identified in the screen have a role in mediating OIS *in vivo*. First, we tested whether they were induced in livers transduced with oncogenic Nras ($Nras^{G12V}$). We observed an increase in *Entpd7*, *Slc31a2* and *Ndst2* expression by $Nras^{G12V}$ in an Arid1b-dependent fashion (Fig. 6A; Supplemental Fig. S7A), suggesting that the coordinated regulation of multiple SWI/SNF-dependent genes could mediate the effects of Arid1b on senescence.

To test this, we examined whether Entpd7 and Slc31a2 mediate OIS *in vivo.* We focused on these two genes because they are downregulated in a large subset of human HCCs (Supplemental Fig. S7B) and their depletion blunted senescence strongly *in vitro*. We transduced mice with vectors co-expressing oncogenic Nras ($Nras^{G12V}$) and a control shRNA or shRNAs targeting Arid1b, Entpd7 or Slc31a2 (Fig. 6B, left). Knockdown of Entpd7 or Slc31a2 resulted in increased numbers of

Nras$^+$ hepatocytes 6 days after transduction (Fig. 6B middle; Supplemental Fig. S7C). Moreover knocking down Entpd7 or Slc31a2 led to an increase in the proportion of Nras$^+$ hepatocytes that were proliferating, suggesting bypass of senescence (Fig. 6B, right). However, the effects observed upon depletion of either Entpd7 or Slc31a2 were not as pronounced as those observed upon Arid1b depletion (Fig. 6B), perhaps because Arid1b regulates multiple targets to control senescence.

To explore this hypothesis, we devised a modified version of the HDTV injection assay that combined transduction of two transposon vectors with the more active SB100 transposase to make possible the simultaneous downregulation of two genes (Fig. 6C). We tested the effect that the combined knockdown of Entpd7 and Slc31a2 had on OIS of hepatocytes *in vivo*, by comparing the results with knockdown of Arid1b (Fig. 6D; Supplemental Fig. S7D). In this assay, individual knockdown of Entpd7 or Slc31a2 caused a modest increase in the percentage of Nras$^+$ hepatocytes present 9 days after transduction. There was a more clear increase in the percentage of proliferating Ki67$^+$/Nras$^+$ hepatocytes upon individual knockdown of Entpd7 or Slc31a2, but it was not comparable to that observed upon Arid1b knockdown in the same setting (Fig. 6D). Interestingly, the combined depletion of Entpd7 and Slc31a2 resulted in an increased proportion of Nras$^+$ and Ki67$^+$/Nras$^+$ hepatocytes, comparable to that observed upon Arid1b knockdown (Fig. 6D). A similar trend was observed when analysing senescence by SA-β-Gal staining. The combined knockdown of Entpd7 and Slc31a2 resulted in a significant decrease of senescence similar to that achieved upon Arid1b downregulation (Fig. 6D). Overall, these results confirm that ARID1B controls senescence by coordinating the regulation of multiple targets.

Nucleotide metabolism is a potential liability of ARID1B-mutant tumours.

Given the prominent tumour suppressor role of senescence, strategies aimed to re-activate senescence in tumours (so-called pro-senescence therapies) have been explored to target cancer (Nardella et al. 2011; Acosta and Gil 2012). As depletion of ARID1B prevents senescence, we postulated that senescence reactivation could be used to target SWI/SNF-mutant tumours. Amongst the ARID1B targets mediating senescence, ENTPD7 was of particular relevance, as it is an enzyme involved in nucleotide catabolism (Shi et al. 2001). Shortage of deoxyribonucleotides (dNTPs) has been previously shown to cause OIS, via activation of DDR (Aird et al. 2013). Interestingly, a significant correlation exists between the expression levels of ENTPD7 and ARID1B in several cancer types, including liver cancer (Supplemental Fig. S8A,B). Moreover, when HCC cases were stratified according to the mutational status of ARID1B or the SWI/SNF complex, we observed significant lower ENTPD7 expression in the mutated samples (Fig. 7A).

Ectopic expression of ENTPD7 in IMR90 cells caused growth arrest and senescence (Fig. 7B,C). ENTPD7 expression induced several senescent effectors, including $p16^{INK4a}$ but more significantly p53 and $p21^{CIP1a}$ and increased DNA damage (Fig. 7D). ENTPD7 belongs to the ENTPD family of ectonucleoside triphosphate diphosphohydrolases. Despite the name, membrane topology analysis predicts that some ENTPDs, such as ENTPD5 and ENTPD7, will reside inside cells and not at their surface (Robson et al. 2006). Therefore, these ENTPDs could affect the intracellular pools of nucleotides, as previously showed for ENTPD5 (Fang et al. 2010).

To investigate the localisation of ENTPD7, given the lack of reliable antibodies, we generated an HA-tagged ENTPD7 version. ENTPD7 localised intracellularly to the Golgi apparatus (Fig. 7E; Supplemental Fig. S8D), in contrast to ENTPD5 that has been described to reside in the ER (Fang et al. 2010). In agreement with its localization, ENTPD7 expression resulted in decreased intracellular dNTP levels in IMR90 cells (Fig. 7F; Supplemental Fig. S8E). Conversely, ENTPD7 knockdown prevented the decrease of dNTPs levels observed during OIS (Fig. 7G; Supplemental Fig. S8F). Interestingly, ectopic expression of ARID1B also ffected dNTP levels (particularly dTTP and dATP) in a similar way to ENTPD7 (Fig. 7F,G; Supplemental Fig. S8E,F). Consistent with this, IPA analysis suggested an association between ARID1B expression and pyrimidine metabolism (Supplemental Fig. S8C).

Based on these observations, we decided to test whether nucleotide metabolism could constitute a liability of ARID1B-deficient cells and potentially of SWI/SNF mutated tumours (Supplemental Fig. S9A). We expressed ENTPD7 in IMR90 ER:RAS cells infected with a control vector or shRNAs targeting ARID1B or p53 (Supplemental Fig. S9B). Expression of ENTPD7 significantly affected the growth of ARID1B-depleted but not p53-depleted cells. The experiment suggested that targeting nucleotide metabolism could be a liability of ARID1B-depleted cells. To directly test this possibility, we took advantage of 6-Diazo-5-oxo-L-norleucine (DON) and Gemcitabine, two drugs inhibiting nucleotide metabolism (Barclay et al. 1962; Wang et al. 2009). Treatment with 5 μM DON did not affect the growth of IMR90 ER:RAS control cells or p53-depleted cells, but significantly arrested ARID1B-depleted cells (Fig. 7H). Similar effects were observed when cells were treated with 5 μM Gemcitabine (Supplemental Fig. S9C). Importantly, the growth arrest in

ARID1B-depleted cells was associated with induction of senescence (Fig. 7I), suggesting that targeting nucleotide metabolism could be used as a prospective pro-senescence therapy against ARID1B-mutant tumours

DISCUSSION

Sequencing cancer genomes is providing us with precise information on the recurrent genetic alterations present in different tumour types. Despite this progress, our knowledge on how some of these mutations affect cancer has not advanced at a similar rate due to the lack of functional information. Since bypass of senescence is a common feature of cancers, we interrogated the ability of genes frequently deleted in HCC to regulate senescence.

In a genetic screen, we identified the SWI/SNF component ARID1B as a regulator of senescence. Other members of the SWI/SNF complex have been previously linked with senescence, including SNF5, BRD7 and BRG1 (Oruetxebarria et al. 2004; Chai et al. 2005; Burrows et al. 2010; Drost et al. 2010). Interestingly, ablation of ARID1B *in vivo* prevents OIS, results in increased proliferation of hepatocytes expressing oncogenic $Nras^{G12V}$ and cooperates in oncogenic transformation. Regulation of $p16^{INK4a}$ and $p21^{CIP1}$ are two suggested mechanisms by which SWI/SNF complexes control senescence (Oruetxebarria et al. 2004; Chai et al. 2005). In addition to downregulating the expression of both CDK inhibitors, manipulating ARID1B levels also affects oxidative stress and DDR. Taking this in consideration, we screened for additional ARID1B-targets mediating senescence. Our results suggest that SWI/SNF induces senescence not only by controlling $p16^{INK4a}$ and $p21^{CIP1}$ expression but also via the coordinated regulation of other genes, including ENTPD7, SLC31A2 and NDST2. Notably, these three novel regulators of senescence identified here have in common that by affecting DDR or oxidative stress could contribute to the activation of the p53/p21 axis.

Due to the high frequency of mutations on SWI/SNF components, there is a strong interest in developing therapies to target these cancers. Studies looking into vulnerabilities of ARID1A- and BRG1-mutant cancers have proposed to target residual SWI/SNF complexes in what has been termed 'cancer-selective paralog dependency' (Helming et al. 2014b; Hoffman et al. 2014). Other therapies for ARID1A-mutated cancers include inhibition of EZH2 (Bitler et al. 2015), PI3K (Samartzis et al. 2014; Bitler et al. 2015) or PARP (Shen et al. 2015). However, there is still the need to identify therapies that could target the whole spectrum of SWI/SNF mutant tumours. Recently, treatments that invoke a senescence response (so-called pro-senescence therapies) have been tested against several tumour types (Nardella et al. 2011; Acosta and Gil 2012). Since senescence is central to the tumour suppressor properties of SWI/SNF, we took advantage of the gained mechanistic insights explaining how ARID1B regulates senescence to target ARID1B-depleted cells. Amongst the ARID1B targets, we singled out ENTPD7, an enzyme involved in nucleotide metabolism. Nucleotide metabolism has been previously linked with DDR activation and ultimately OIS (Aird et al. 2013). Cells with reduced ARID1B expression underwent a strong senescence arrest in response to ENTPD7 expression or treatment with inhibitors of nucleotide metabolism (Fig. 7). It could be argued that this response would imply intact p53 signalling. Interestingly, some studies have highlighted mutual exclusivity between SWI/SNF and p53 mutations (Guan et al. 2011; Kadoch et al. 2013). Although the connection between SWI/SNF and p53 is complex, our results suggest a functional overlap between both pathways that could explain their mutual exclusivity in cancer (Supplemental Fig. S9B). In turn, the wild-type p53 status of a significant subset of SWI/SNF-mutant tumours will make them more sensitive to nucleotide metabolism inhibitors.

In conclusion, we have identified *ARID1B* as a gene commonly altered in HCC with the ability to control senescence. Regulation of senescence could explain in part the role of SWI/SNF in tumour suppression. By unveiling novel pathways regulated by SWI/SNF in senescence, our investigation suggests novel therapeutic targets, such as nucleotide metabolism, that could be relevant to treat tumours deficient in *ARID1B* and by extension in other SWI/SNF components.

MATERIALS AND METHODS

Cell culture, retroviral and lentiviral Infection

HEK-293T and IMR90 cells were obtained from the ATCC. MEFs were prepared as described in the Supplemental Information. Cell lines were grown and infected with retroviral or lentiviral vectors as described in the Supplemental Information.

BrdU incorporation, crystal violet staining and SA-β-galactosidase staining

These procedures have been previously described (Banito et al. 2009; Barradas et al. 2009; Debacq-Chainiaux et al. 2009; Acosta et al. 2013).

Soft agar assay

Ras^{V12G} infected MEFs were suspended in complete DMEM containing 0.35% agar (Sigma) and seeded in triplicate on 6-well plates pre-coated with 0.7% agar in complete growth medium and incubated at 37°C, 5% CO_2. After 21 days, colonies were photographed and counted in 10 randomly chosen fields.

Gene expression analysis

Total RNA was extracted using Trizol reagent (Invitrogen) and the RNeasy isolation kit (Qiagen). cDNAs were generated using SuperScript II reverse transcriptase (Invitrogen), dNTPs and Random Hexamers. PCR reactions were performed in a Real-Time PCR Detection System (BioRad) using Power SYBR Green Master Mix or TaqMan Universal PCR Master Mix (Applied Biosystems). Expression was normalized to ribosomal protein S14 (*RPS14*) expression. Primer sets used are listed in Table S3. Mice tissue samples were weighed and ground to a fine powder in liquid nitrogen. The RNA was then extracted and processed as described above.

In vivo senescence and tumourigenesis experiments

For all animal experiments, only mice in a C57BL/6 background were used (equal gender distribution in randomized groups). C57BL/6 mice were purchased from Charles River. At day 0 hydrodynamic tail vein injection of a transposon-based Nras expression plasmid together with an expression plasmid for the sleeping beauty 13 was performed, as described in details before (Kang et al. 2011). Animals were sacrificed and livers collected at specific timepoints (day 6 and 9) or, in the tumourigenesis study, when termination criteria were fulfilled. Samples were fixed and subjected to IHC analysis as described in the Supplemental Information. The antibodies used are listed in Table S4. No statistical method was used to predetermine sample size. The investigators were not blinded to allocation during experiments and outcome assessment. All mice were maintained under specific pathogen-free conditions in accordance with the institutional guidelines of the University of Tübingen. The German legal authorities approved these experiments.

Immunofluorescence and high content analysis

IF was performed as previously described (Banito et al. 2009) using the antibodies listed in Table S4. Details of high content analysis, immunofluorescence in mouse tissue and confocal microscopy are provided in the Supplemental Information.

Statistical analysis

All statistical analysis were performed by two-tailed Student *t*-test unless stated otherwise.

ACKNOWLEDGEMENTS

We are grateful to S. Lowe and all members of J. Gil's laboratory for reagents, helpful comments and contributions to this project. This project was supported in part by an MRC Centenary Award. R. García-Escudero was funded by grant ISCIII-RETIC RD12/0036/0009. Core support from MRC (grants MC-A652-5PZ00 and MC_U120085810) funded the research in J. Gil's laboratory.

REFERENCES

Acosta JC, Banito A, Wuestefeld T, Georgilis A, Janich P, Morton JP, Athineos D, Kang TW, Lasitschka F, Andrulis M et al. 2013. A complex secretory program orchestrated by the inflammasome controls paracrine senescence. *Nat Cell Biol* **15**: 978-990.

Acosta JC, Gil J. 2012. Senescence: a new weapon for cancer therapy. *Trends Cell Biol* **22**: 211-219.

Aird KM, Zhang G, Li H, Tu Z, Bitler BG, Garipov A, Wu H, Wei Z, Wagner SN, Herlyn M et al. 2013. Suppression of nucleotide metabolism underlies the establishment and maintenance of oncogene-induced senescence. *Cell Rep* **3**: 1252-1265.

Banito A, Rashid ST, Acosta JC, Li S, Pereira CF, Geti I, Pinho S, Silva JC, Azuara V, Walsh M et al. 2009. Senescence impairs successful reprogramming to pluripotent stem cells. *Genes Dev* **23**: 2134-2139.

Barclay RK, Garfinkel E, Phillipps MA. 1962. Effects of 6-diazo-5-oxo-L-norleucine on the incorporation of precursors into nucleic acids. *Cancer research* **22**: 908-914.

Barradas M, Anderton E, Acosta JC, Li S, Banito A, Rodriguez-Niedenfuhr M, Maertens G, Banck M, Zhou MM, Walsh MJ et al. 2009. Histone demethylase JMJD3 contributes to epigenetic control of INK4a/ARF by oncogenic RAS. *Genes Dev* **23**: 1177-1182.

Bitler BG, Aird KM, Garipov A, Li H, Amatangelo M, Kossenkov AV, Schultz DC, Liu Q, Shih Ie M, Conejo-Garcia JR et al. 2015. Synthetic lethality by targeting EZH2 methyltransferase activity in ARID1A-mutated cancers. *Nat Med* **21**: 231-238.

Burrows AE, Smogorzewska A, Elledge SJ. 2010. Polybromo-associated BRG1-associated factor components BRD7 and BAF180 are critical regulators of p53 required for induction of replicative senescence. *Proc Natl Acad Sci U S A* **107**: 14280-14285.

Chai J, Charboneau AL, Betz BL, Weissman BE. 2005. Loss of the hSNF5 gene concomitantly inactivates p21CIP/WAF1 and p16INK4a activity associated with replicative senescence in A204 rhabdoid tumor cells. *Cancer Res* **65**: 10192-10198.

Cheng SW, Davies KP, Yung E, Beltran RJ, Yu J, Kalpana GV. 1999. c-MYC interacts with INI1/hSNF5 and requires the SWI/SNF complex for transactivation function. *Nat Genet* **22**: 102-105.

Collado M, Serrano M. 2010. Senescence in tumours: evidence from mice and humans. *Nature reviews Cancer* **10**: 51-57.

Debacq-Chainiaux F, Erusalimsky JD, Campisi J, Toussaint O. 2009. Protocols to detect senescence-associated beta-galactosidase (SA-betagal) activity, a biomarker of senescent cells in culture and in vivo. *Nat Protoc* **4**: 1798-1806.

Drost J, Mantovani F, Tocco F, Elkon R, Comel A, Holstege H, Kerkhoven R, Jonkers J, Voorhoeve PM, Agami R et al. 2010. BRD7 is a candidate tumour suppressor gene required for p53 function. *Nat Cell Biol* **12**: 380-389.

Fang M, Shen Z, Huang S, Zhao L, Chen S, Mak TW, Wang X. 2010. The ER UDPase ENTPD5 promotes protein N-glycosylation, the Warburg effect, and proliferation in the PTEN pathway. *Cell* **143**: 711-724.

Fellmann C, Hoffmann T, Sridhar V, Hopfgartner B, Muhar M, Roth M, Lai DY, Barbosa IA, Kwon JS, Guan Y et al. 2013. An optimized microRNA backbone for effective single-copy RNAi. *Cell Rep* **5**: 1704-1713.

Fujimoto A, Totoki Y, Abe T, Boroevich KA, Hosoda F, Nguyen HH, Aoki M, Hosono N, Kubo M, Miya F et al. 2012. Whole-genome sequencing of liver cancers identifies etiological influences on mutation patterns and recurrent mutations in chromatin regulators. *Nat Genet* **44**: 760-764.

Guan B, Wang TL, Shih Ie M. 2011. ARID1A, a factor that promotes formation of SWI/SNF-mediated chromatin remodeling, is a tumor suppressor in gynecologic cancers. *Cancer research* **71**: 6718-6727.

Hanahan D, Weinberg RA. 2011. Hallmarks of cancer: the next generation. *Cell* **144**: 646-674.

Helming KC, Wang X, Roberts CW. 2014a. Vulnerabilities of mutant SWI/SNF complexes in cancer. *Cancer Cell* **26**: 309-317.

Helming KC, Wang X, Wilson BG, Vazquez F, Haswell JR, Manchester HE, Kim Y, Kryukov GV, Ghandi M, Aguirre AJ et al. 2014b. ARID1B is a specific vulnerability in ARID1A-mutant cancers. *Nat Med* **20**: 251-254.

Hoffman GR, Rahal R, Buxton F, Xiang K, McAllister G, Frias E, Bagdasarian L, Huber J, Lindeman A, Chen D et al. 2014. Functional epigenetics approach identifies BRM/SMARCA2 as a critical synthetic lethal target in BRG1-deficient cancers. *Proceedings of the National Academy of Sciences of the United States of America* **111**: 3128-3133.

Jacobs JJ, Keblusek P, Robanus-Maandag E, Kristel P, Lingbeek M, Nederlof PM, van Welsem T, van de Vijver MJ, Koh EY, Daley GQ et al. 2000. Senescence bypass screen identifies TBX2, which represses Cdkn2a (p19(ARF)) and is amplified in a subset of human breast cancers. *Nat Genet* **26**: 291-299.

Kadoch C, Hargreaves DC, Hodges C, Elias L, Ho L, Ranish J, Crabtree GR. 2013. Proteomic and bioinformatic analysis of mammalian SWI/SNF complexes identifies extensive roles in human malignancy. *Nat Genet* **45**: 592-601.

Kang TW, Yevsa T, Woller N, Hoenicke L, Wuestefeld T, Dauch D, Hohmeyer A, Gereke M, Rudalska R, Potapova A et al. 2011. Senescence surveillance of pre-malignant hepatocytes limits liver cancer development. *Nature*.

Khursheed M, Kolla JN, Kotapalli V, Gupta N, Gowrishankar S, Uppin SG, Sastry RA, Koganti S, Sundaram C, Pollack JR et al. 2013. ARID1B, a member of the human SWI/SNF chromatin remodeling complex, exhibits tumour-suppressor activities in pancreatic cancer cell lines. *Br J Cancer* **108**: 2056-2062.

Kia SK, Gorski MM, Giannakopoulos S, Verrijzer CP. 2008. SWI/SNF mediates polycomb eviction and epigenetic reprogramming of the INK4b-ARF-INK4a locus. *Mol Cell Biol* **28**: 3457-3464.

Kondoh H, Lleonart ME, Gil J, Wang J, Degan P, Peters G, Martinez D, Carnero A, Beach D. 2005. Glycolytic enzymes can modulate cellular life span. *Cancer Res* **65**: 177-185.

Kuilman T, Michaloglou C, Mooi WJ, Peeper DS. 2010. The essence of senescence. *Genes Dev* **24**: 2463-2479.

Lee D, Kim JW, Seo T, Hwang SG, Choi EJ, Choe J. 2002. SWI/SNF complex interacts with tumor suppressor p53 and is necessary for the activation of p53-mediated transcription. *J Biol Chem* **277**: 22330-22337.

Lee JJ, Sholl LM, Lindeman NI, Granter SR, Laga AC, Shivdasani P, Chin G, Luke JJ, Ott PA, Hodi FS et al. 2015. Targeted next-generation sequencing reveals high frequency of mutations in epigenetic regulators across treatment-naive patient melanomas. *Clinical epigenetics* **7**: 59.

Nardella C, Clohessy JG, Alimonti A, Pandolfi PP. 2011. Pro-senescence therapy for cancer treatment. *Nature reviews Cancer* **11**: 503-511.

Narita M, Lowe SW. 2005. Senescence comes of age. *Nat Med* **11**: 920-922.

Oruetxebarria I, Venturini F, Kekarainen T, Houweling A, Zuijderduijn LM, Mohd-Sarip A, Vries RG, Hoeben RC, Verrijzer CP. 2004. P16INK4a is required for hSNF5 chromatin remodeler-induced cellular senescence in malignant rhabdoid tumor cells. *J Biol Chem* **279**: 3807-3816.

Plass C, Pfister SM, Lindroth AM, Bogatyrova O, Claus R, Lichter P. 2013. Mutations in regulators of the epigenome and their connections to global chromatin patterns in cancer. *Nat Rev Genet* **14**: 765-780.

Robson SC, Sevigny J, Zimmermann H. 2006. The E-NTPDase family of ectonucleotidases: Structure function relationships and pathophysiological significance. *Purinergic Signal* **2**: 409-430.

Samartzis EP, Gutsche K, Dedes KJ, Fink D, Stucki M, Imesch P. 2014. Loss of ARID1A expression sensitizes cancer cells to PI3K- and AKT-inhibition. *Oncotarget* **5**: 5295-5303.

Sausen M, Leary RJ, Jones S, Wu J, Reynolds CP, Liu X, Blackford A, Parmigiani G, Diaz LA, Jr., Papadopoulos N et al. 2013. Integrated genomic analyses identify ARID1A and ARID1B alterations in the childhood cancer neuroblastoma. *Nat Genet* **45**: 12-17.

Shain AH, Pollack JR. 2013. The spectrum of SWI/SNF mutations, ubiquitous in human cancers. *PLoS One* **8**: e55119.

Shen J, Peng Y, Wei L, Zhang W, Yang L, Lan L, Kapoor P, Ju Z, Mo Q, Shih Ie M et al. 2015. ARID1A Deficiency Impairs the DNA Damage Checkpoint and Sensitizes Cells to PARP Inhibitors. *Cancer discovery* **5**: 752-767.

Shi JD, Kukar T, Wang CY, Li QZ, Cruz PE, Davoodi-Semiromi A, Yang P, Gu Y, Lian W, Wu DH et al. 2001. Molecular cloning and characterization of a novel mammalian endo-apyrase (LALP1). *J Biol Chem* **276**: 17474-17478.

Trouche D, Le Chalony C, Muchardt C, Yaniv M, Kouzarides T. 1997. RB and hbrm cooperate to repress the activation functions of E2F1. *Proc Natl Acad Sci U S A* **94**: 11268-11273.

Wang J, Lohman GJ, Stubbe J. 2009. Mechanism of inactivation of human ribonucleotide reductase with p53R2 by gemcitabine 5'-diphosphate. *Biochemistry* **48**: 11612-11621.

Watson IR, Takahashi K, Futreal PA, Chin L. 2013. Emerging patterns of somatic mutations in cancer. *Nat Rev Genet* **14**: 703-718.

Wilson BG, Roberts CW. 2011. SWI/SNF nucleosome remodellers and cancer. *Nat Rev Cancer* **11**: 481-492.

Zender L, Xue W, Zuber J, Semighini CP, Krasnitz A, Ma B, Zender P, Kubicka S, Luk JM, Schirmacher P et al. 2008. An oncogenomics-based in vivo RNAi screen identifies tumor suppressors in liver cancer. *Cell* **135**: 852-864.

FIGURE LEGENDS

Figure 1. An shRNA screen identifies the SWI/SNF subunit ARID1B as a regulator of senescence. (A) Schematic model of the bypass of senescence screen using a library of shRNAs targeting genes deleted in HCC. An average of 2 different shRNAs per gene were used. MEFs were infected with the shRNA library or controls and passaged until vector cells reached senescence. shRNAs that extended lifespan were recovered by Next Generation Sequencing (NGS). The screen was performed in triplicate. (B) List of significantly enriched shRNAs by Fisher's combined p value ($p < 0.001$). shRNAs targeting ARID1B are marked in red. (C) Representative images of ARID1B, BrdU, senescent-associated-β-galactosidase (SA-β-Gal) immunofluorescence (IF) staining and colony formation assay (crystal violet) of MEFs transduced with shRNAs targeting ARID1B, $p16^{INK4a}$ or empty vector. DAPI was used to visualize the nuclei. Scale bar, 30 μm. Quantification of IF by high content analysis (HCA) is shown on the right. (D) Soft agar assay of MEFs transduced with Ras^{G12V} cDNA and either an empty vector or vectors carrying shRNAs for p16/Arf or ARID1B. Representative images at 4X magnification (left) and quantification (right) are shown. Graphs in C and D represent mean ± SD from *n=4* and *n=3*, respectively. $^{***}p < 0.001$ by two-tailed Student *t*-test.

Figure 2. Knockdown of *Arid1b* alleviates OIS *in vivo* and cooperates in HCC formation. (A) Scheme of the *in vivo* senescence experiments. Transposon constructs carrying $Nras^{G12V}$ cDNA and ARID1B shRNAs (or control) were delivered into mouse livers by hydrodynamic injection ($Nras^{G12V/D38A}$ was used as negative

control). *n*=4 mice per condition were used. (B) Quantification of ARID1B nuclear IF staining in $Nras^{+}$ mouse hepatocytes in the above-described conditions is shown. (C) Representative pictures of immunohistochemistry (IHC) for Nras, SA-β-Gal staining and IF staining for $p21^{CIP1}$ and $p16^{INK4a}$ on liver sections from mice injected with the indicated vectors. (D-F) Quantification of the SA-β-Gal staining, percentages of Nras-, $p16^{INK4a}$- or $p21^{CIP1}$-positive cells (D) and 53BP1- (E) or Ki67-positive cells (F) in liver sections from mice injected with the indicated vectors. Graphs represent mean ± SD from *n=4* mice. $^{***}p < 0.001$; $^{**}p < 0.01$; $^{*}p < 0.05$; n.s. non significant by two-tailed Student *t*-test. (G) Scheme of the *in vivo* tumour growth experiment (left). Transposon constructs carrying $Nras^{G12V}$ cDNA and an ARID1B shRNA (or control) were delivered into mouse livers by hydrodynamic injection. Mice were monitored for 30 weeks. *n*=10 (shCTR) and n=13 (shArid1b.1) mice were used. Kaplan-Meier survival curves (left) and representative pictures of livers (right) showing GFP-positive tumour nodules, as they were derived from the injected constructs. $^{*}p < 0.05$ by Long-rank (Mantel-Cox) test. Scale bar 100 μm C. DAPI was used to visualize the nuclei.

Figure 3. ARID1B regulates oncogene-induced senescence in human cells. (A) IMR90 ER:RAS cells were transduced with either an empty vector (vec, vector), a p53 shRNA (shp53) or ARID1B shRNAs (shA2, shARID1B.2; shA3, shARID1B.3) and induced to undergo senescence by 4OHT treatment. (A) Cell proliferation was assessed by crystal violet staining (top left) and BrdU incorporation (right). Senescence was measured by SA-β-Gal staining (representative pictures on bottom left and quantification on the right). (B) IMR90 ER:RAS transduced with an empty vector (± 4OHT) or ARID1B shRNAs (+ 4OHT) were subjected to global mRNA

expression analysis (left). Data were subjected to gene set enrichment analysis (GSEA) and Ingenuity Pathway Analysis (IPA). *n=3* biological replicates were used. GSEA showing loss of a signature associated with OIS in the gene expression profile of IMR90 ER:RAS shARID1B versus empty vector, both 4OHT treated (middle). NES, normalized enriched score; FDR, false discovery rate. IPA upstream regulator analysis of the indicated comparisons is shown (right). The predicted activation (z-score) of SMARCA4, TP53 and ROS pathways is shown. (C-D) Quantification by HCA (D) of IF staining for $p21^{CIP1}$, $p16^{INK4a}$, p53, γH2AX and 8-oxodG (C) in IMR90 ER:RAS cells transduced with either an empty vector or an shRNA targeting ARID1B (± 4OHT). DAPI was used to visualize the nuclei. Graphs represent mean ± SD from *n*=4 (A, BrdU) and *n*=3 (A, SA-β-Gal and D). $^{***}p < 0.001$; $^{**}p < 0.01$; $^{*}p < 0.05$ by two-tailed Student *t*-test. Scale bars, 30 μm.

Figure 4. Ectopic expression of ARID1B induces senescence. (A and D-E) IMR90 cells were transduced either with an empty vector, *ARID1B* cDNA or Ras^{G12V} cDNA and then analysed for cell growth (crystal violet), SA-β-Gal activity, BrdU incorporation (A) and IF staining using the indicated antibodies (D). DAPI was used to visualize the nuclei. (E) Quantification by HCA of IF staining in D. Data represents mean ± SD from *n=3* (A, SA-β-Gal) and *n=4* (A, BrdU and E). (B) RNA-Seq was performed with IMR90 cells transduced with either an empty vector or *ARID1B* cDNA. Data were subjected to GSEA and IPA analysis. *n*=3 biological replicates were used. (C) IPA upstream regulator analysis of the RNA-seq reveals activation (z-score) of SMARCA4, TP53 and ROS pathways. (F) IMR90 cells were co-transduced with an empty vector or *ARID1B* cDNA and shRNAs targeting $p21^{CIP1}$,

$p16^{INK4a}$ or p53. Cell proliferation was assessed by crystal violet staining. $^{***}p < 0.001$; $^{**}p < 0.01$ by two-tailed Student *t*-test. Scale bars, 30 μm.

Figure 5. A focused shRNA screen identifies novel ARID1B effectors controlling senescence. (A) Schematic model of the bypass of senescence screen using a library of shRNAs targeting genes upregulated in OIS, including some ARID1B-dependent. An average of six different shRNAs per gene were used. After infection with the shRNA library or controls IMR90 ER:RAS were treated with 4OHT and passaged until library-infected cells bypassed senescence. shRNAs that bypassed senescence were recovered by NGS. The screen was performed in duplicate. (B) List of significantly enriched genes by Fisher's combined p value ($p < 0.001$). *CDKN1A and g*enes selected for further analysis are marked in red. (C-E) Colony formation assay (C), BrdU incorporation (D) and p21 analysis (E) of IMR90 co-transduced with Ras^{G12V} (or empty vector) and shRNAs for ENTPD7 (shE2, shE3), SLC31A2 (shS1, shS2) or NDST2 (shN1, shN2). A p53 shRNA was used as control. Quantifications of IF staining were performed by HCA (*n=3*). Graphs represents mean ± SD. $^{***}p < 0.001$; $^{**}p < 0.005$; $^{*}p < 0.05$ by two-tailed Student *t*-test.

Figure 6. ARID1B controls senescence by coordinated regulation of multiple targets. (A) $Nras^{G12V}$ or $Nras^{G12V/D38A}$ transposon constructs were delivered into mouse livers by hydrodynamic injection. Livers were harvested after six days, followed by mRNA extraction and qRT-PCR analysis for *Entpd7*, *Slc31a2* and *Ndst2* mRNA levels. *n=6* mice per condition were used. (B) Transposon constructs carrying $Nras^{G12V}$ cDNA and shRNAs targeting ARID1B (shAR.1), ENTPD7

(shEN.1; shEN.2), SLC31A2 (shSL.1; shSL.2) or control (shCTR) were delivered into mouse livers by hydrodynamic injection. *n=4* mice per condition were used. Livers were harvested after six days and sections were stained for Nras and Ki67. Quantification of IF staining is shown on the right. Graphs represent mean ± SD. $^{***}p < 0.001$; $^{**}p < 0.005$; $^{*}p < 0.05$; n.s. non significant by two-tailed Student *t*-test. (E) Transposon constructs carrying $Nras^{G12V}$ cDNA and combinations of two control shRNAs, one control and one targeting ARID1B (shAR.1), one control and one targeting ENTPD7 (shEN.1), one control and one targeting SLC31A2 (shSL.2) and a combination of ENTPD7 and SLC31A2 shRNAs (shEN.1+shSL.2) were delivered into mouse livers by hydrodynamic injection. In this experiment, a more active transposase (SB100) that allows integration of multiple shRNAs, was used. *n=3* mice per condition were used. Livers were harvested after nine days and sections were stained for Nras, Ki67 and SA-β-Gal. Representative pictures of IHC for Nras and SA-β-Gal staining are shown. Quantification of the staining is shown at the bottom. Scale bar, 100 μm. Graphs represents mean ± SD. $^{***}p < 0.001$; $^{**}p < 0.005$; $^{*}p < 0.05$; n.s. non-significant by two-tailed Student *t*-test.

Figure 7. ARID1B deficient cells are sensitive to alterations in nucleotide pathway. (A) ENTPD7 differential expression between SWI/SNF or ARID1B mutant/wild type samples was calculated using Student's *t*-test (details in methods) using the TCGA LIHC dataset. (B) Colony formation assay (top), SA-β-Gal staining (middle), and BrdU IF (bottom) of IMR90 transduced with an empty vector or cDNA of *ARID1B* or *ENTPD7*. Scale bar, 30 μm. (C) Quantification by HCA of BrdU IF and SA-β-Gal staining is shown (*n=3*). (D) Quantification by HCA of IF staining for p53, $p21^{CIP1}$, $p16^{INK4a}$, 8-oxodG and γH2AX in IMR90 cells transduced with *ENTPD7*

cDNA or empty vector (*n=3*). (E) Representative images of HA-tag IF staining of IMR90 cells transduced either with an empty vector or an HA-tagged *ENTPD7* cDNA. DAPI was used to visualize the nuclei. Scale bar, 10 μm. (F) IMR90 cells were transduced either with an empty vector, *ARID1B* cDNA or *ENTPD7* cDNA and then intracellular dNTP levels were measured. (G) IMR90 ER:RAS cells were transduced with either an empty vector, an ARID1B shRNA or an ENTPD7 shRNA and induced to undergo senescence by 4OHT treatment (+). Intracellular dNTP levels were measured 5 days after 4OHT. (H-I) Cell growth assay (H, crystal violet) and SA-β-Gal staining (I) of stable ARID1B-knockdown, p53-knockdown or control IMR90 ER:RAS cells treated with 4OHT, followed by DON (5 μM) or DMSO. For H and I: left, representative images; right, quantification. Graphs represent mean ± SD from *n*=2 (H) and *n*=3 (F, G and I). $^{***}p < 0.001$; $^{**}p < 0.005$; $^{*}p < 0.05$; n.s. non-significant by two-tailed Student *t*-test.

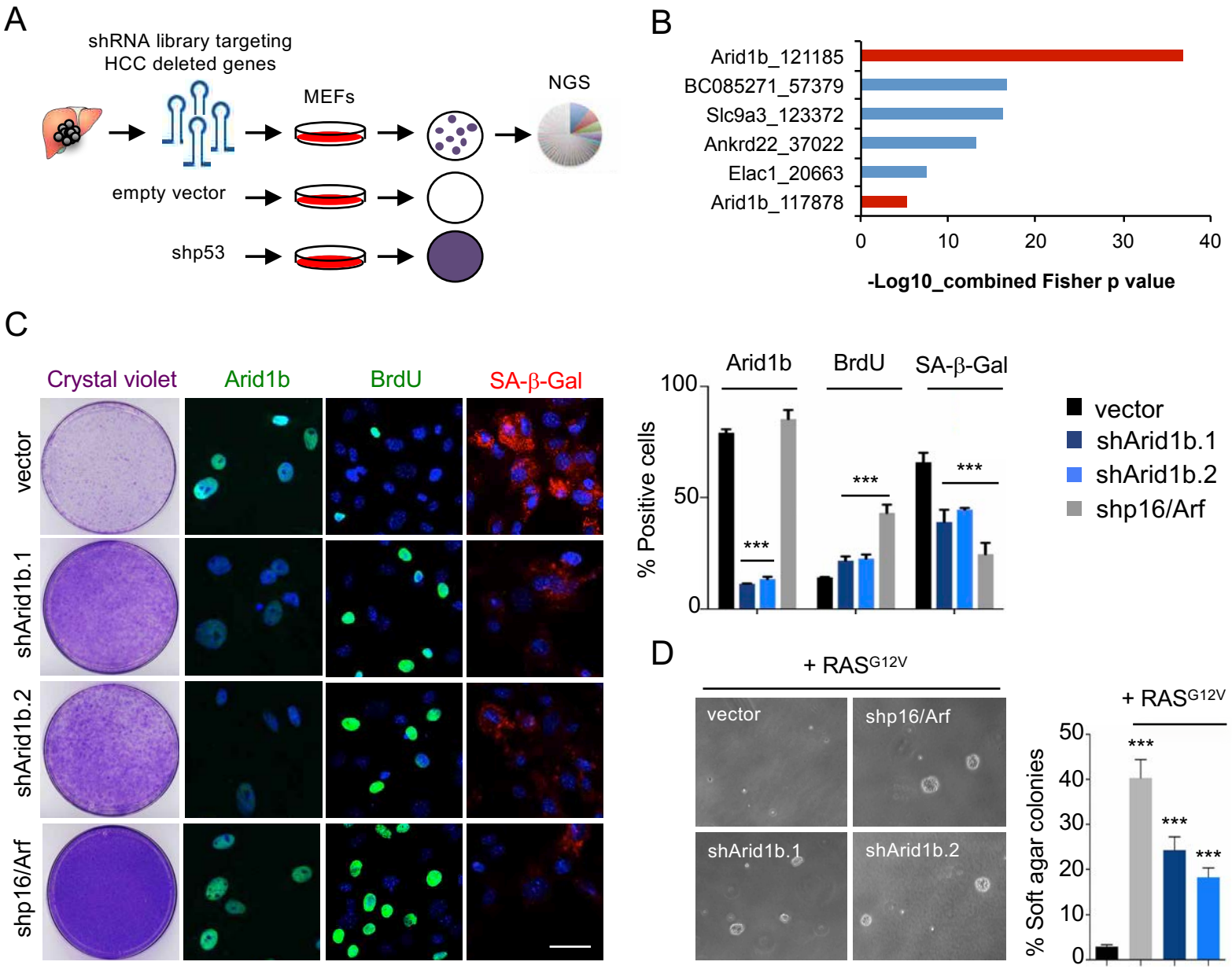
A
shRNA library targeting
HCC deleted genes
MEFs
NGS
empty vector
shp53
B
Arid1b_121185
BC085271_57379
Slc9a3_123372
Ankrd22_37022
Elac1_20663
Arid1b_117878
0
10
20
30
40
-Log10_combined Fisher p value
C
Crystal violet
Arid1b
BrdU
SA-β-Gal
vector
shArid1b.1
shArid1b.2
shp16/Arf
Arid1b
BrdU
SA-β-Gal
100
50
0
% Positive cells
***
***
***
vector
shArid1b.1
shArid1b.2
shp16/Arf
D
+ RASG12V
vector
shp16/Arf
shArid1b.1
shArid1b.2
+ RASG12V
50
40
30
20
10
0
% Soft agar colonies
***
***
***

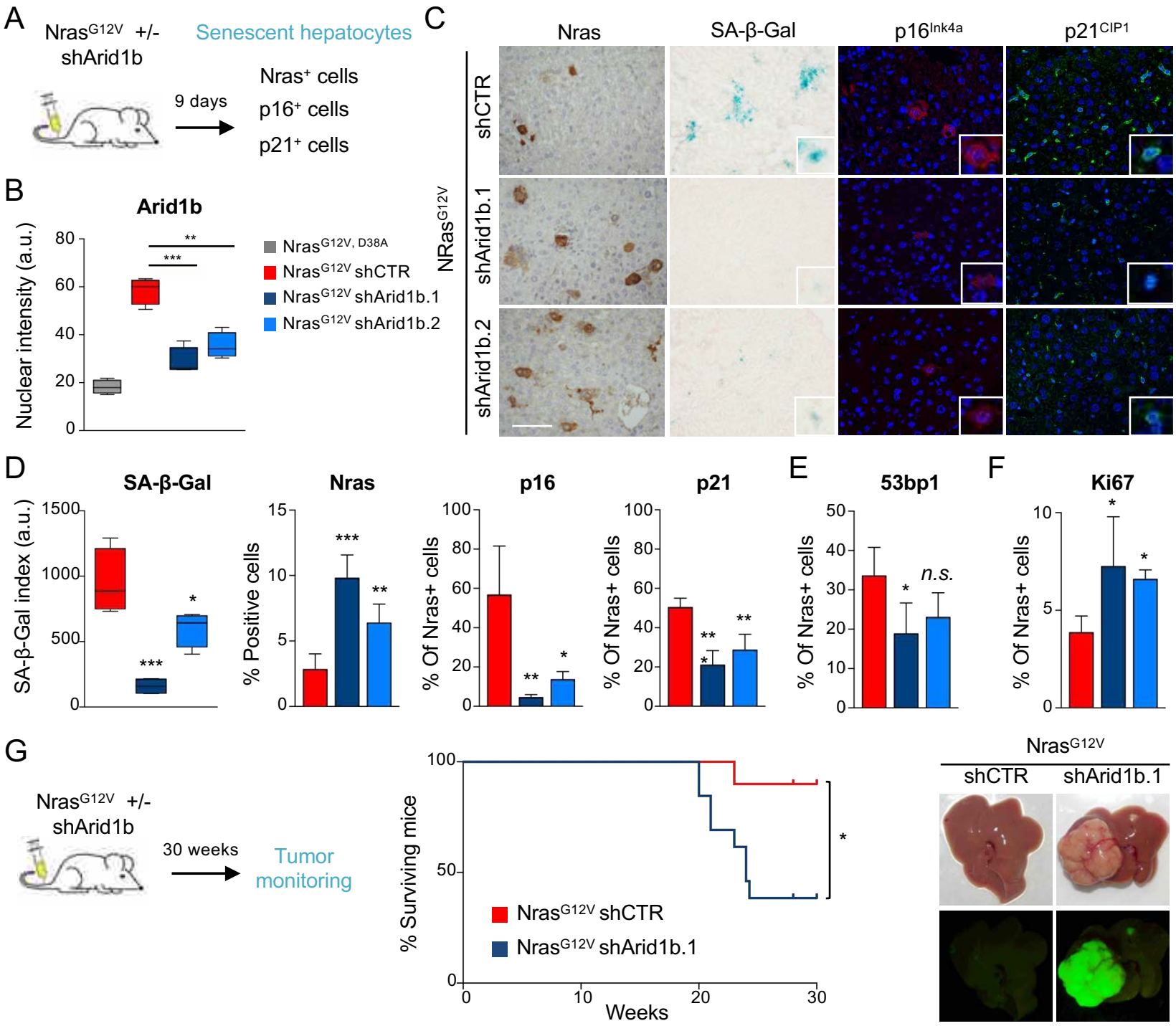
A
NrasG12V +/-
shArid1b
9 days
Senescent hepatocytes
Nras+ cells
p16+ cells
p21+ cells
B
Arid1b
Nuclear intensity (a.u.)
NrasG12V, D38A
NrasG12V shCTR
NrasG12V shArid1b.1
NrasG12V shArid1b.2
C
Nras
SA-β-Gal
p16Ink4a
p21CIP1
shCTR
shArid1b.1
shArid1b.2
NRasG12V
D
SA-β-Gal
SA-β-Gal index (a.u.)
Nras
% Positive cells
p16
% Of Nras+ cells
p21
% Of Nras+ cells
E
53bp1
% Of Nras+ cells
n.s.
F
Ki67
% Of Nras+ cells
G
NrasG12V +/-
shArid1b
30 weeks
Tumor
monitoring
% Surviving mice
NrasG12V shCTR
NrasG12V shArid1b.1
Weeks
NrasG12V
shCTR
shArid1b.1

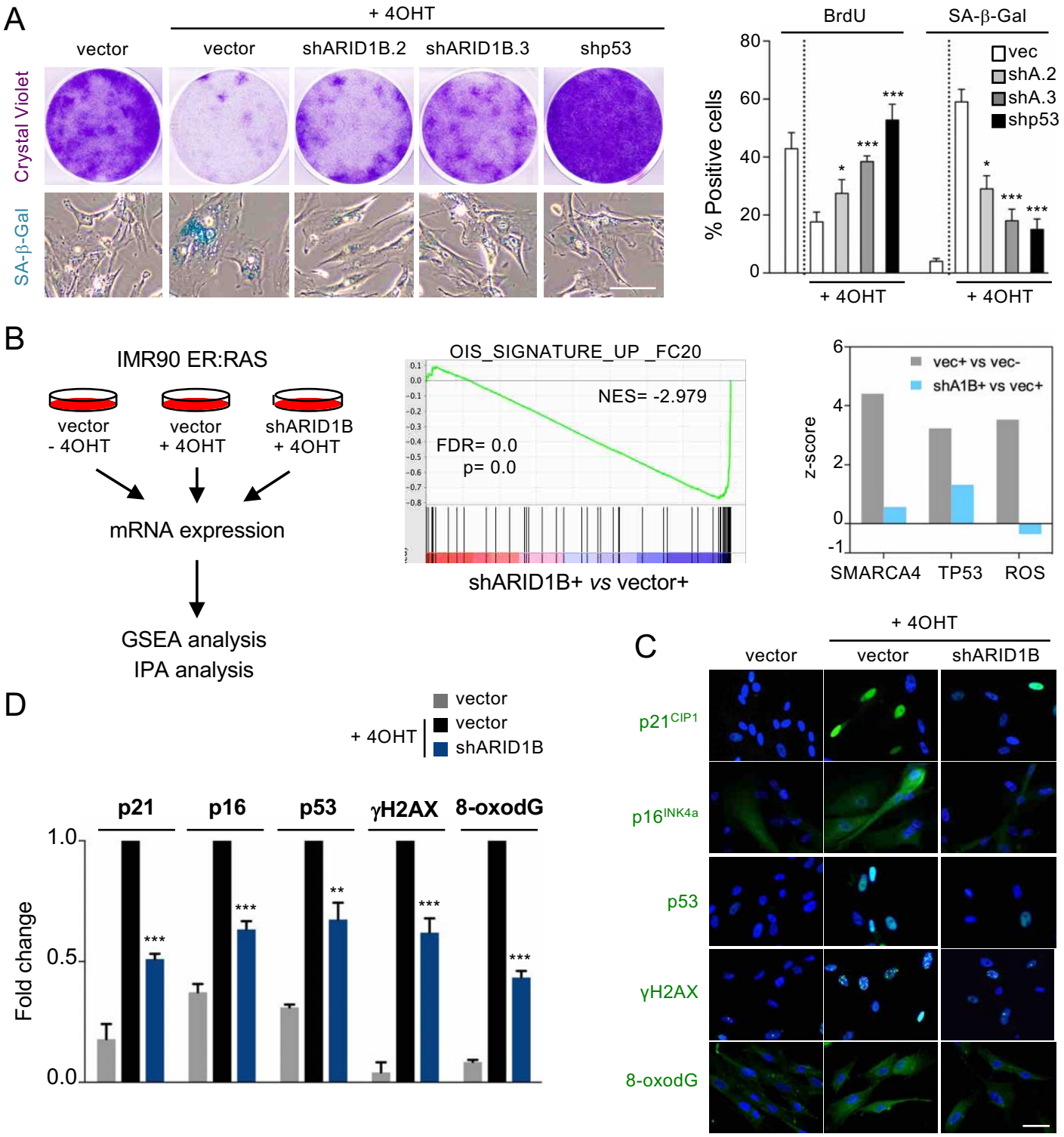
A
+ 4OHT
vector
vector
shARID1B.2
shARID1B.3
shp53
Crystal Violet
SA-β-Gal
BrdU
SA-β-Gal
% Positive cells
vec
shA.2
shA.3
shp53
+ 4OHT
+ 4OHT
B
IMR90 ER:RAS
vector
- 4OHT
vector
+ 4OHT
shARID1B
+ 4OHT
mRNA expression
GSEA analysis
IPA analysis
OIS_SIGNATURE_UP _FC20
NES= -2.979
FDR= 0.0
p= 0.0
shARID1B+ vs vector+
vec+ vs vec-
shA1B+ vs vec+
z-score
SMARCA4
TP53
ROS
C
+ 4OHT
vector
vector
shARID1B
p21CIP1
p16INK4a
p53
γH2AX
8-oxodG
D
vector
vector
shARID1B
+ 4OHT
p21
p16
p53
γH2AX
8-oxodG
Fold change

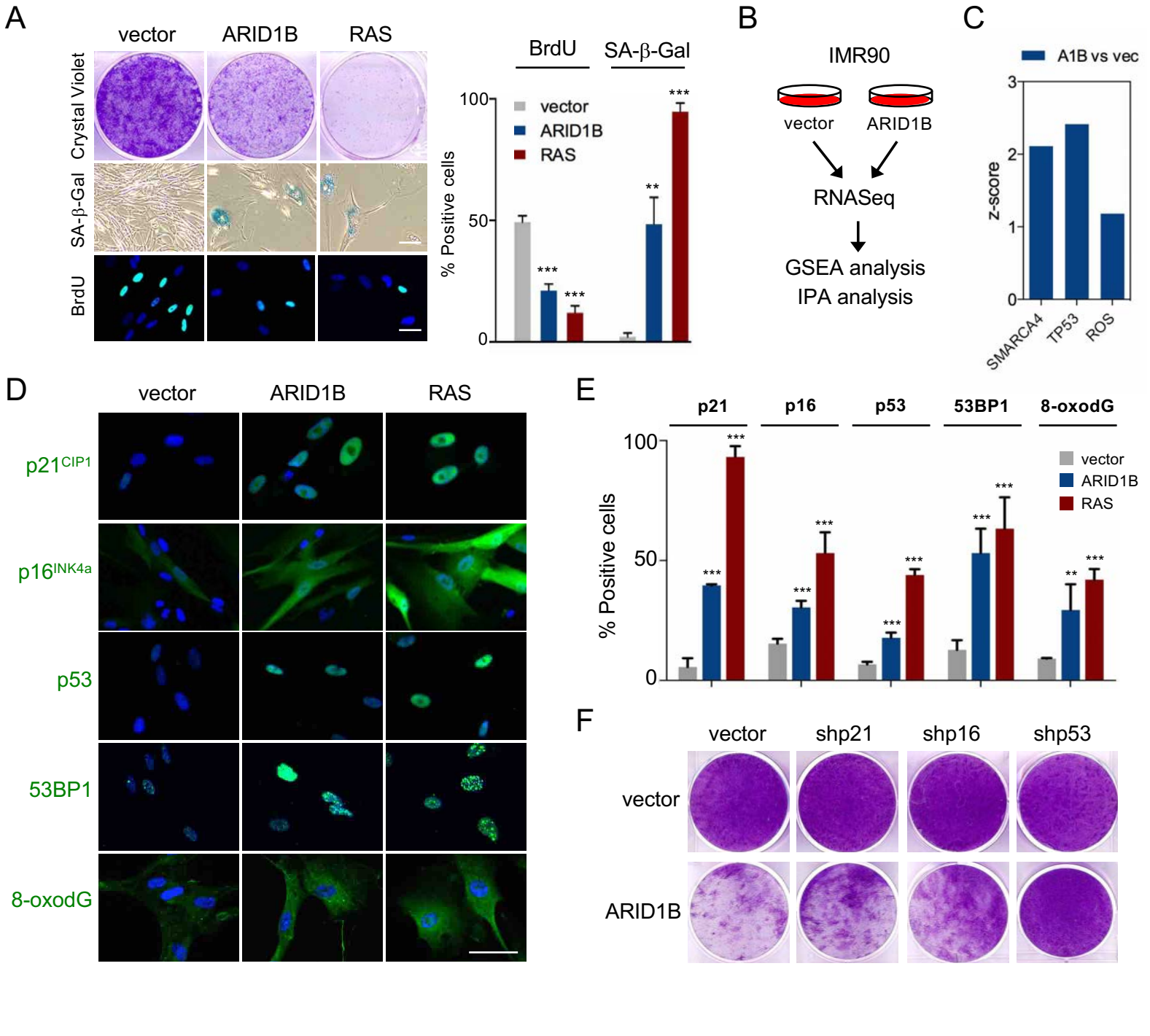
A
vector
ARID1B
RAS
Crystal Violet
SA-β-Gal
BrdU
BrdU
SA-β-Gal
% Positive cells
100
50
0
vector
ARID1B
RAS
***
***
**
***
B
IMR90
vector
ARID1B
RNASeq
GSEA analysis
IPA analysis
C
A1B vs vec
z-score
3
2
1
0
SMARCA4
TP53
ROS
D
vector
ARID1B
RAS
p21CIP1
p16INK4a
p53
53BP1
8-oxodG
E
p21
p16
p53
53BP1
8-oxodG
% Positive cells
100
50
0
vector
ARID1B
RAS
F
vector
shp21
shp16
shp53
vector
ARID1B

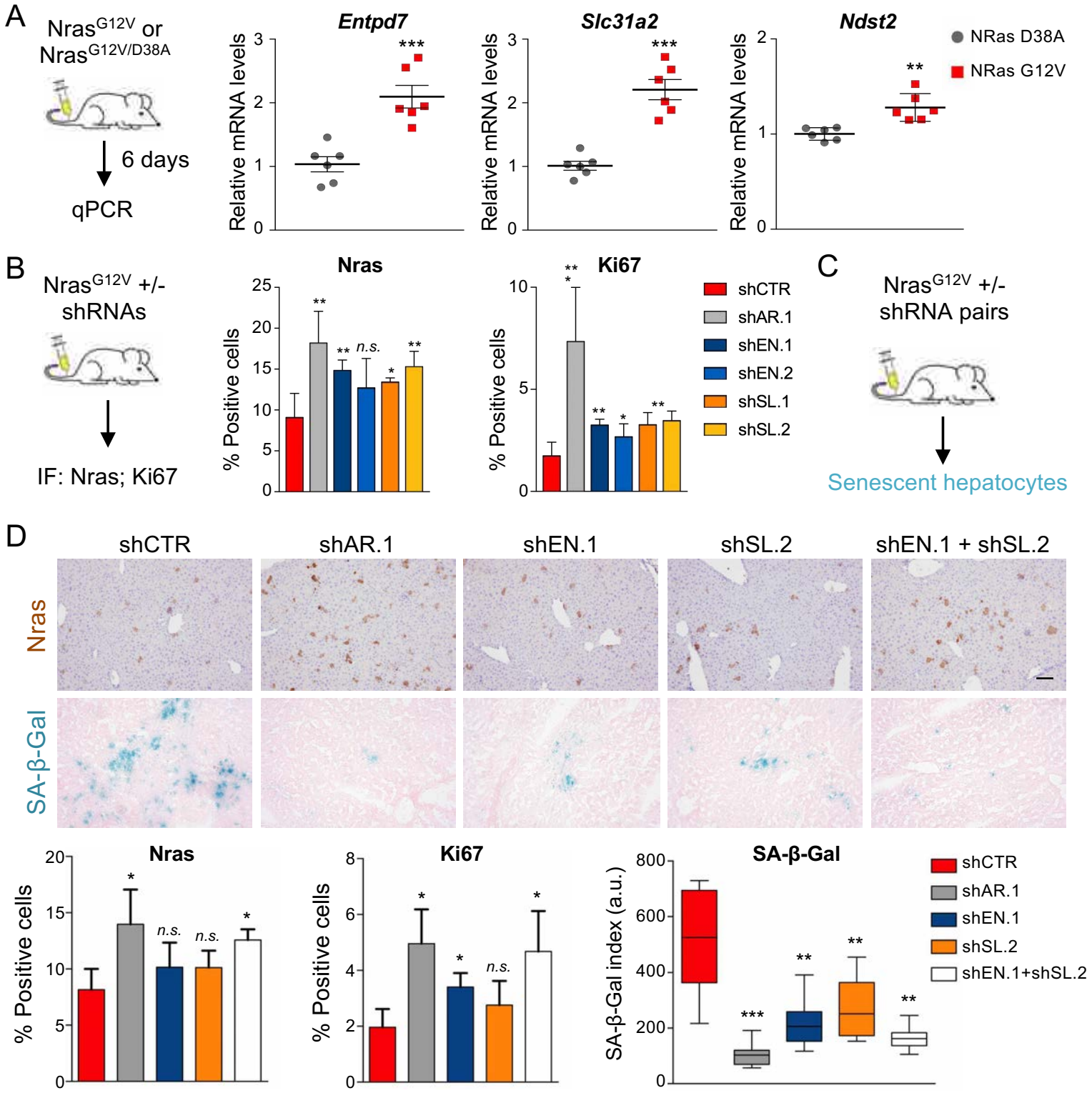
A
Nras^G12V or Nras^G12V/D38A
6 days
qPCR
Entpd7
Slc31a2
Ndst2
Relative mRNA levels
NRas D38A
NRas G12V
B
Nras^G12V +/- shRNAs
IF: Nras; Ki67
Nras
Ki67
% Positive cells
shCTR
shAR.1
shEN.1
shEN.2
shSL.1
shSL.2
C
Nras^G12V +/- shRNA pairs
Senescent hepatocytes
D
shCTR
shAR.1
shEN.1
shSL.2
shEN.1 + shSL.2
Nras
SA-β-Gal
Nras
Ki67
SA-β-Gal
SA-β-Gal index (a.u.)
shCTR
shAR.1
shEN.1
shSL.2
shEN.1+shSL.2

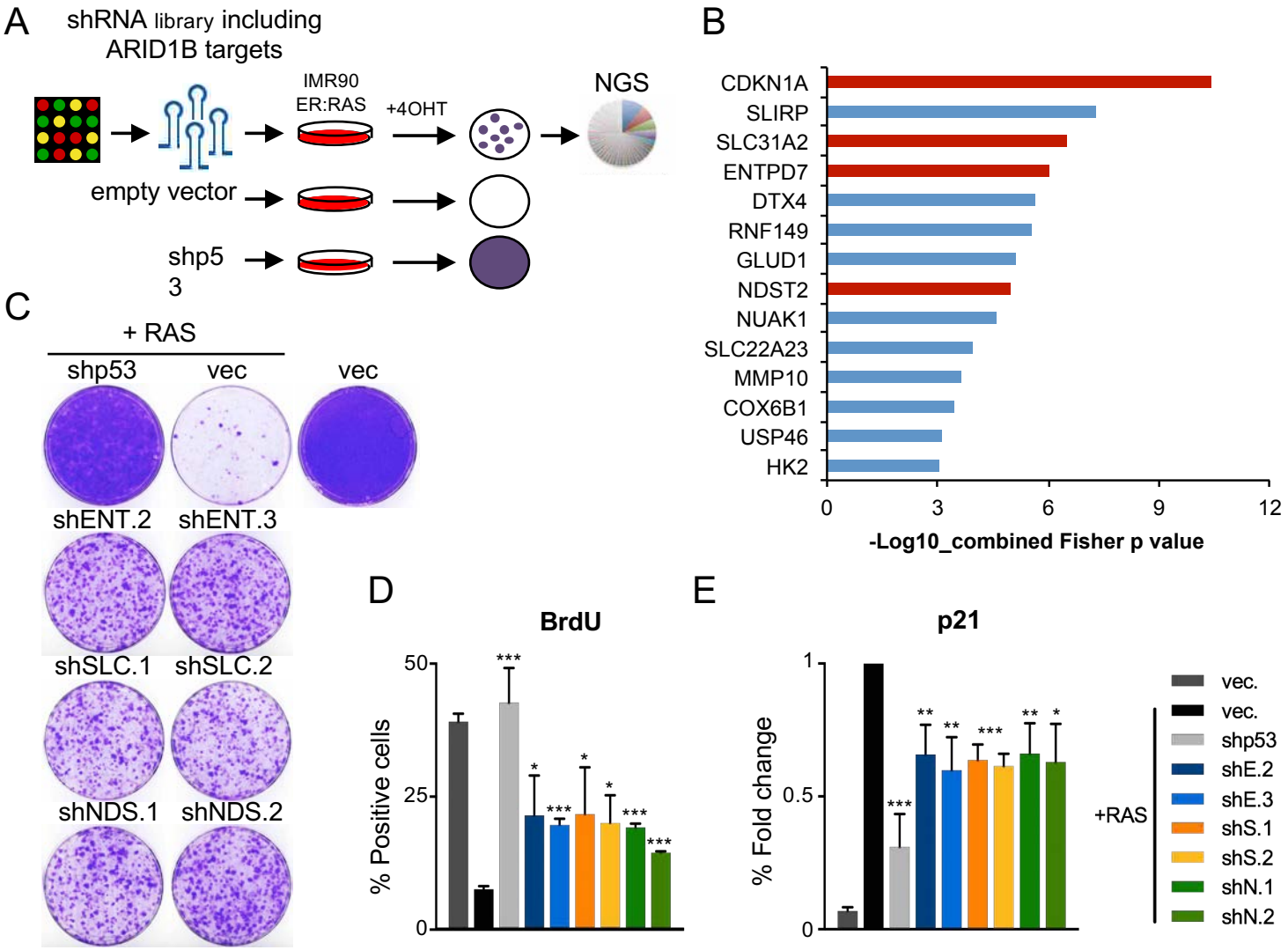
A
shRNA library including
ARID1B targets
IMR90
ER:RAS
+4OHT
NGS
empty vector
shp5
3
B
CDKN1A
SLIRP
SLC31A2
ENTPD7
DTX4
RNF149
GLUD1
NDST2
NUAK1
SLC22A23
MMP10
COX6B1
USP46
HK2
0
3
6
9
12
-Log10_combined Fisher p value
C
+ RAS
shp53
vec
vec
shENT.2
shENT.3
shSLC.1
shSLC.2
shNDS.1
shNDS.2
D
BrdU
% Positive cells
50
25
0
E
p21
% Fold change
1
0.5
0
+RAS
vec.
vec.
shp53
shE.2
shE.3
shS.1
shS.2
shN.1
shN.2

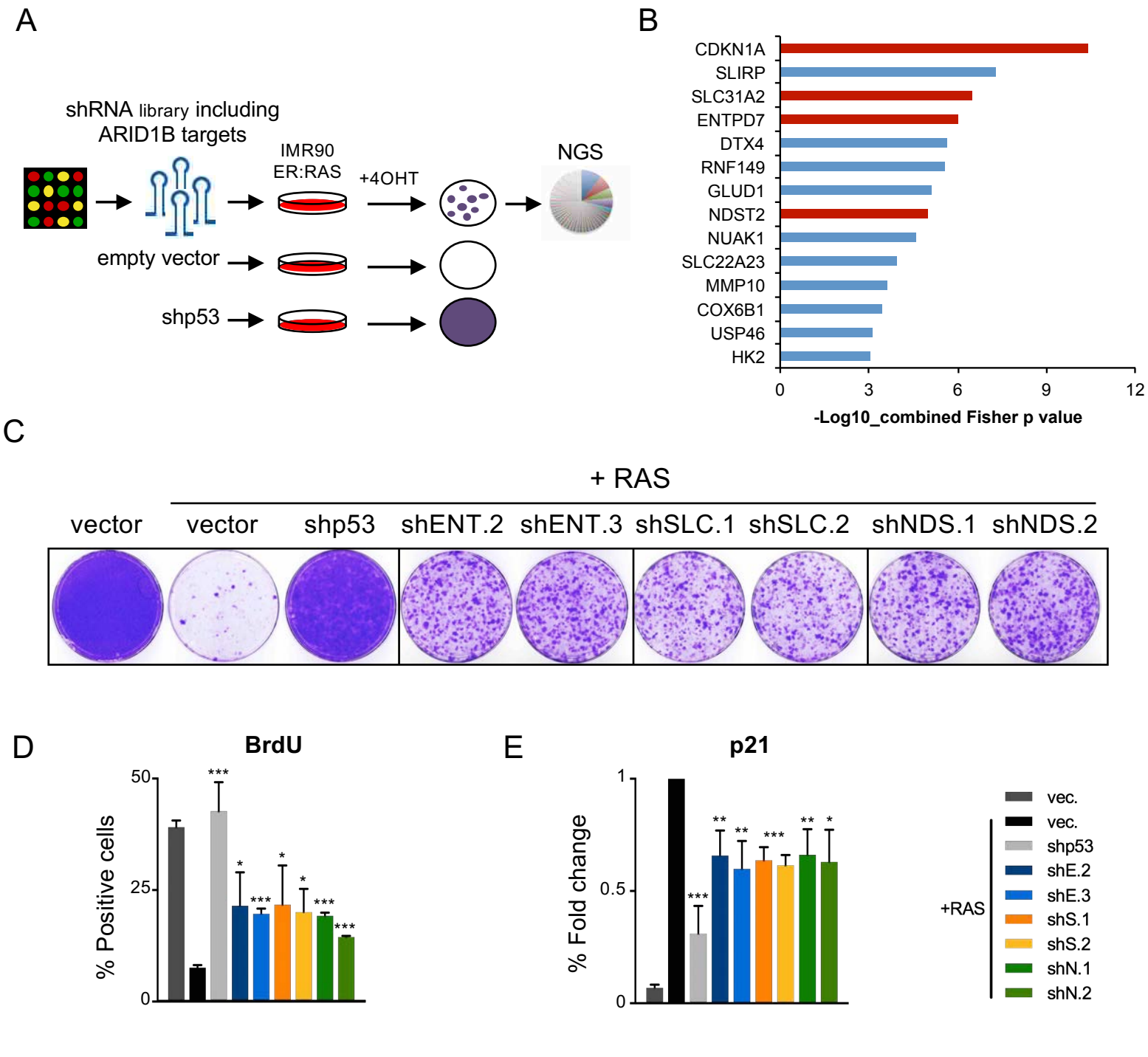
A
shRNA library including
ARID1B targets
IMR90
ER:RAS
+4OHT
NGS
empty vector
shp53
B
CDKN1A
SLIRP
SLC31A2
ENTPD7
DTX4
RNF149
GLUD1
NDST2
NUAK1
SLC22A23
MMP10
COX6B1
USP46
HK2
0
3
6
9
12
-Log10_combined Fisher p value
C
+ RAS
vector
vector
shp53
shENT.2
shENT.3
shSLC.1
shSLC.2
shNDS.1
shNDS.2
D
BrdU
% Positive cells
50
25
0
E
p21
% Fold change
1
0.5
0
vec.
vec.
shp53
shE.2
shE.3
shS.1
shS.2
shN.1
shN.2
+RAS

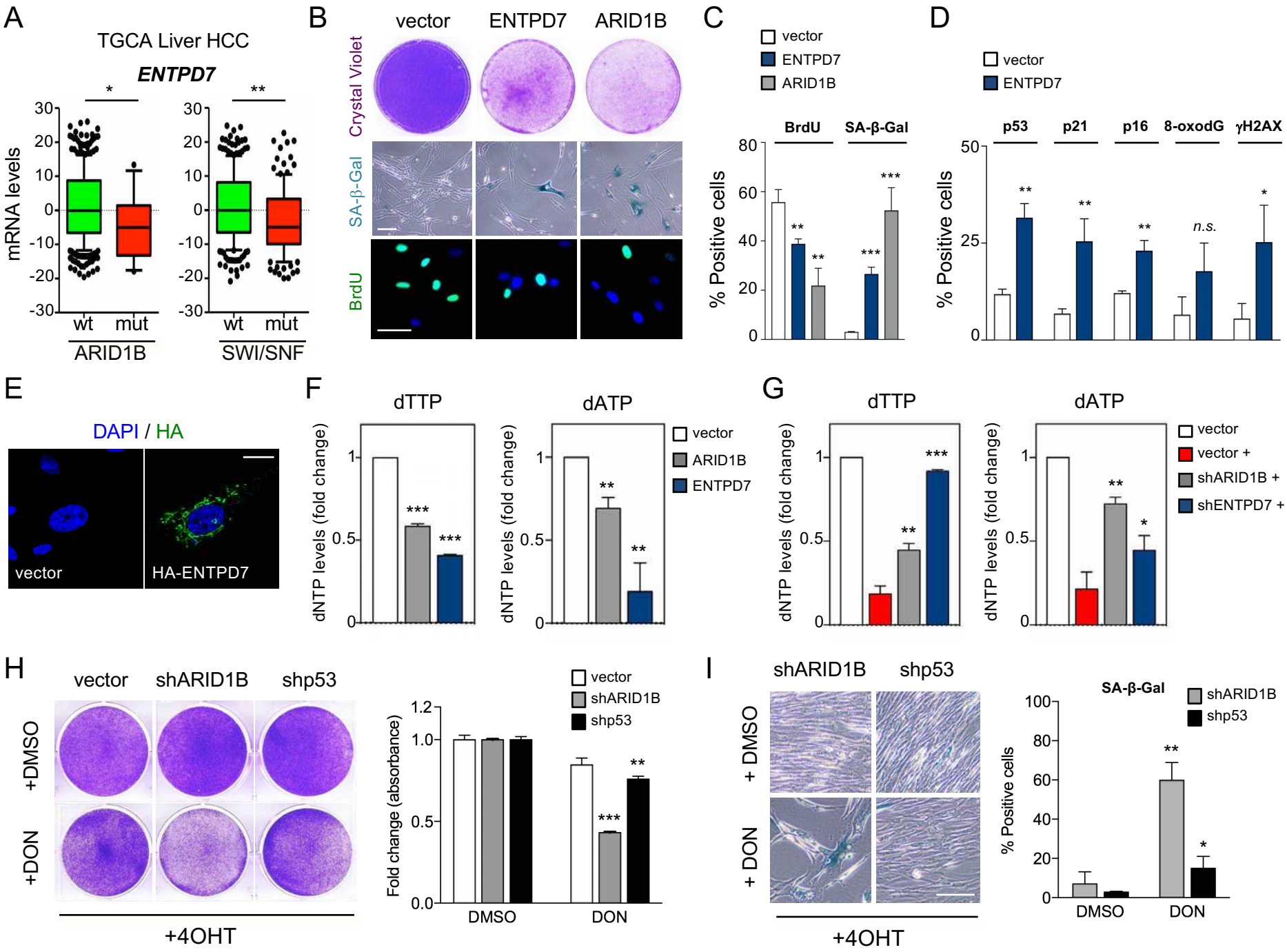
A
TGCA Liver HCC
ENTPD7
mRNA levels
wt
mut
ARID1B
SWI/SNF
B
vector
ENTPD7
ARID1B
Crystal Violet
SA-β-Gal
BrdU
C
vector
ENTPD7
ARID1B
BrdU
SA-β-Gal
% Positive cells
D
vector
ENTPD7
p53
p21
p16
8-oxodG
γH2AX
n.s.
% Positive cells
E
DAPI / HA
vector
HA-ENTPD7
F
dTTP
dATP
dNTP levels (fold change)
vector
ARID1B
ENTPD7
G
dTTP
dATP
dNTP levels (fold change)
vector
vector +
shARID1B +
shENTPD7 +
H
vector
shARID1B
shp53
+DMSO
+DON
+4OHT
Fold change (absorbance)
DMSO
DON
I
shARID1B
shp53
+ DMSO
+ DON
+4OHT
SA-β-Gal
% Positive cells
DMSO
DON